Thermally propagated Al contacts on SiGe nanowires characterized by electron beam induced current in a scanning transmission electron microscope

Aidan Conlan, Minh Anh Luong, Pascal Gentile, Grigore Moldovan, Martien den Hertog, Eva Monroy, David Cooper

Thermally propagated Al contacts on SiGe nanowires characterized by electron beam induced current in a scanning transmission electron microscope

Aidan P Conlan*[1], Minh Anh Luong[2], Pascal Gentile[3], Grigore Moldovan[4], Martien I den Hertog[2], Eva Monroy[3] and David Cooper[1]

[1] Univ. Grenoble Alpes, CEA-LETI, F-38000 Grenoble, France

[2] Univ. Grenoble Alpes, CNRS-Institut Néel, 25 avenue des Martyrs, F-38000 Grenoble, France

[3] Univ. Grenoble Alpes, CEA, Grenoble INP, IRIG, PHELIQS, 17 av. des Martyrs, F-38000 Grenoble, France

[4] point electronic GmbH, Erich-Neuss-Weg 15, D-06120 Halle (Saale), Germany

Abstract

Here, we use electron beam induced current in a scanning transmission electron microscope to characterize the structure and electronic properties of Al/SiGe and Al/Si-rich/SiGe axial nanowire heterostructures fabricated by thermal propagation of Al in a SiGe nanowire. The two heterostructures behave as Schottky contacts with different barrier heights. From the sign of the beam induced current collected at the contacts, the intrinsic semiconductor doping is determined

to be *n*-type. Furthermore, we find that the silicon-rich double interface presents a lower barrier height than the atomically sharp SiGe/Al interface. With an applied bias, the Si-rich region delays the propagation of the depletion region and presents a reduced free carrier diffusion length with respect to the SiGe nanowire. This behaviour could be explained by a higher residual doping in the Si-rich area. These results demonstrate that STEM EBIC is a powerful method for mapping and quantifying electric fields in micrometer- and nanometer-scale devices.

Keywords: Nanowires, EBIC, TEM, SiGe.

1. Introduction

Nanowires (NWs) are well positioned to play an important role in solar energy harvesting due to their high relative surface area and tolerance for strained structures such as multiple quantum wells.[1] To fully exploit this advantage, minimization of the contact resistance with high quality contacts is required. Recently it has been demonstrated that, upon heating, a metal can propagate along a silicon or germanium NW creating a metal/semiconductor/metal NW axial heterostructure with controlled dimensions.[2–8] Depending on the natures of the metal and semiconductor, the metal propagates as a pure element or as a metal silicide/germanide. It has been shown in the Al/Ge system that a thermally induced exchange reaction occurs[9], forming an atomically abrupt contact between a monocrystalline Al NW section that propagated in the original NW volume, and the original Ge NW.[7] Such an abrupt and clean contact contained within the NW has many uses, such as a gate electrode that is not screened by the contacts. Studies have been extended to Si_xGe_{1-x} NWs, where thermal propagation of aluminium results in Al/SiGe/Al heterostructures with atomically sharp interfaces.[10]

Atomic resolution structural characterization of NW heterostructures is now routine by transmission electron microscopy[11,12] and advances in lithographic contacting methods allow individual nanowires to be electrically characterized[13]. Electron beam induced current (EBIC) combines electron microscopy and *in situ* electrical biasing, enabling direct correlation of the positions and strengths of electric fields with micro- or nano-scale structural features.[14,15] This is usually achieved in a scanning electron microscope (SEM) with beam energies in the range of 2 – 20 kV.[16–19] However, even in low dimensional materials such as nanowires, the generation of charge carriers in SEM is not uniform with depth and spreads laterally, degrading the spatial resolution of the technique. Careful modelling of the generation volume is required to deconvolve its shape and density distribution from the EBIC map[20–22], especially in complex geometries such as nanowires, where the size of the generation volume is comparable to the specimen dimensions[23–27]. Scanning transmission electron microscopy (STEM) EBIC[28–33] uses a high energy beam in the range of 80 - 300 kV to form a localized generation volume which is uniform through the thickness of the nanowire, greatly simplifying the interpretation of the EBIC maps. This is only possible as the high energy incident electrons are not absorbed by the specimen, unlike low energy electrons in SEM. This also allows complementary STEM techniques such as high angle annular dark field (HAADF) and bright field (BF) imaging to be implemented in tandem.

We demonstrate the first STEM EBIC analysis of a nanowire and quantify the properties of the electric fields at the metal – semiconductor interfaces, and use it to explain the macroscopic properties as measured in the current-voltage response.[34] The method is applied to an Al/SiGe/Al axial NW heterostructure obtained by thermal propagation of Al into a SiGe NW. Such contacts are very well suited for (STEM) EBIC studies due to their shape. In typical contact geometries the metal is present on top of the NW, and therefore any effect of the contact first penetrates into the

NW volume, before it can extends axially. In the present contact geometry, any effect of the contact can be observed directly in the adjacent SiGe NW section.

2. Experimental

Our experiments focus on non-intentionally doped $Si_{0.67}Ge_{0.33}$ NWs grown by chemical vapor deposition on a Si(111) substrate, using silane and germane as precursors and gold as catalyst. The NWs were grown along the [111] direction. For observation, the nanowires were dispersed in ethanol, deposited on a home-made electron-transparent silicon nitride membrane, as reported elsewhere[10,35,36]. The nanowires were then coated in a 20-nm-thick Al_2O_3 passivation shell using atomic layer deposition at 250°C. Prior to the deposition of the contacts, the NWs were immersed in a buffered HF solution for 50s to remove the Al_2O_3 shell in the contact regions, rinsed by deionized water and then dipped in diluted HI for 5 s to etch the native GeO_2 shell. The samples were then cleaned by soft Ar plasma and coated by a 200-nm-thick Al layer using electron beam evaporation. Propagation of Al into the wires was activated using rapid thermal annealing (RTA) in a temperature range of 400 to 450°C in N_2 atmosphere. The RTA experiments were performed in a Jipelec™ JetFirst RTP Furnace. The heating initiates a solid-state reaction where Al diffuses into the nanowire, progressively replacing the original SiGe NW and forming a sharp interface with the remaining SiGe section (see figure 1).[5,8,9] In the Al/SiGe NW system, a reversible reaction occurs: upon slow cooling, a Si-rich segment can be created that extends out from the Al/SiGe interface towards the Al contact pad. This partially reversible reaction is described in detail in references[10,36]. Extensive structural and chemical analyses of these NW structures has also been presented in these references, and complementary information is given in Supplementary Material Section 1.

STEM EBIC, or STEBIC, was performed in a FEI Titan Ultimate aberration-corrected (S)TEM microscope operated at 80 kV with a convergence angle of 31 mrad using a point electronic GmbH EBIC system. A system of two amplifiers was connected in series with the nanowire: the first amplifies the signal as it leaves the specimen holder, and the second controls the dynamic range of current collection. 80 kV beam electrons were used to avoid knock-on damage in the SiGe lattice. HAADF and BF images can also be acquired simultaneously with the EBIC data. All images were acquired with a 1 nA beam current, as measured on the TEM phosphor screen, unless otherwise stated. High resolution HAADF STEM images were acquired on a probe corrected Titan Themis operated at 200 kV. A DENSsolutions double tilt six contacts heating/biasing TEM sample holder was used to hold and contact the specimen.

Simulations of high energy electron collisions were calculated using the CASINO Monte Carlo code.[37] The trajectories of 1000 electrons in a 1 nm diameter probe were simulated with an absorption threshold of 50 eV for a SiGe nanowire 150 nm in diameter on a 200 nm-thick SiN membrane.

3. Results and discussion

Figure 1(a) shows a HAADF STEM image of a SiGe nanowire supported on a silicon nitride membrane and contacted with two aluminium pads. The higher magnification inset confirms that aluminium diffused through the nanowire during heating[5,8,10] so that only the centre of the nanowire remains SiGe. The sample was cooled rapidly over 4 minutes after RTA, leading to only a thin Si-rich interlayer, approximately 40 nm wide, at one of the Al/SiGe contacts (left side in figure 1a). No Si-rich region was created at the other SiGe/Al contact (right side in figure 1a), likely due to

small differences at the NW surface, allowing us to compare in a single specimen the electrical properties of Al/Si-rich/SiGe and SiGe/Al contacts.

Nominally-identical NWs (i.e. NWs with thermally-propagated Al contacts following the same process) were suspended on a 40 nm-thick SiN_x membrane so that high-resolution HAADF STEM imaging was possible (figure 1b and c). These atomic-resolution images with Z-contrast show that the Al/Si-rich/SiGe "double interface" is atomically sharp,[7] yet it incorporates an approximately 10 nm-thick silicon-rich region between Al and SiGe.[36] We arbitrarily chose to apply bias to the electrode connected to the double interface and connect the sharp Al/SiGe contact to ground, as illustrated in figure 1a.

Figure 2a shows the current-voltage characteristic of the nanowire under study, measured in the ±4 V range using the point electronic EBIC system. The non-linear behaviour points to the two metal-semiconductor interfaces acting as opposing Schottky contacts. The equivalent circuit of the system has been made using a general opposing diode model[34] fitted to the observed current-voltage characteristic, and is shown in figure 2b. The total current across the nanowire, J, was modelled using:

$$J(V) = \frac{J_1 J_2 \sinh\left(\frac{qV}{2k_B T}\right)}{J_1 \exp\left(\frac{qV}{2k_B T}\right) + J_2 \exp\left(\frac{qV}{2k_B T}\right)} \quad (1)$$

with

$$J_{1,2} = A.T^2 \exp\left(\frac{q\phi_{B1,B2}}{k_B T}\right) \quad (2)$$

and

$$\phi_{B1,B2} = \phi_{B01,B02} + V_{1,2}\left(\frac{1}{n_{1,2}} - 1\right) \quad (3)$$

where V is the applied bias, Φ is the barrier height of the respective junction, n is the ideality factor of the barrier, q is the charge of an electron, k_B is the Boltzmann constant, T is temperature, and A is the Richardson constant.

At a certain bias, the shape of the current-voltage curve of opposing diodes is dominated by whichever diode is conducting. Knowing this, the barrier heights and ideality factors were found to be 0.68 eV and 1.047, respectively, for the Schottky contact that conducts under negative applied bias, and 0.66 eV and 1.076, respectively, for the Schottky contact that conducts under positive applied bias. Typically, Al contacts result in Schottky barrier heights of ≈ 0.8 eV on *p*-Si[38], ≈ 0.7 eV on *p*-Ge [39], up to 0.86 eV on *n*-Si[40] and ≈ 0.7 eV on *n*-Ge[41]. Therefore the obtained barrier height values are within the expected range for Al on SiGe. The leak resistance was 3 GΩ and the series resistance was determined to be 200 kΩ from linear fits of the experimental data around the 0 V and 3-4 V ranges, respectively.

To further explore the behaviour of these metal-semiconductor contacts, we have performed a STEM EBIC study using a focused electron beam with an acceleration voltage of 80 kV. If the electron-hole pairs generated by the incident electron beam diffuse to an area with an electric field, positive and negative charge carriers are separated, and so contribute to the collected current. In this way we can characterize each depletion region and its associated diffusion length, providing that the diffusion lengths are shorter than the distance between contacts. Figure 3a shows 80 kV

electron trajectories in a SiGe nanowire 150 nm in diameter supported on a 200 nm-thick SiN_x substrate. There is little spreading of the trajectories within the nanowire, only in the SiN_x substrate. The wires were found to damage quickly when using a beam energy of 200 kV from knock on effects. There are alternative techniques, such as electron holography, that could be used to measure the potentials in the NWs with high sensitivity. However, SiN_x membranes charge under beam irradiation which leads to uninterpretable results. DPC and pixelated (4D) STEM measure the field directly, but suffer from dynamical charging as the beam is scanned across the region of interest. Additionally, the use of a convergent beam for pixelated STEM leads to results that are much more difficult to interpret than holography, which uses a plane electron wave. As STEM EBIC only collects charge carriers generated in a highly localized volume which is homogenous through the thickness of the nanowire, accurate quantification of electric fields is possible directly from images without requiring the generation volume shape to be simulated.[42] This would not be the case for low energy electrons in a SEM, where the generation volume usually spreads much more laterally and changes through the specimen thickness.

Figure 3b shows a zero-bias STEM EBIC image of the nanowire visualized by HAADF STEM in figure 3c, where the signal originating in the proximity of the two opposing Schottky contacts is clearly resolved. Here we use the conventionally defined direction of positive current, which is indicated in the inset. The sign of the EBIC current provides experimental evidence that the metal contacts induce an upwards band bending in the semiconductor, as expected in the case of a Schottky contact on *n*-type material. Therefore, the direction of the measured current is consistent with the band profile in figure 3d. The band diagram was calculated assuming that the nanowire residual doping is *n* type and the crystal structure is relaxed, so that the Si/SiGe system is a type 2 heterostructure. As a result, the contact following the Si-rich area should present a slightly lower

barrier than the atomically-sharp SiGe/Al interface. Returning to the Schottky barrier heights extracted from the current-voltage characteristics in the dark (figure 1), and observing that the shape of the current-voltage curve is dominated by whichever diode is conducting, we conclude that $\Phi = 0.66$ eV and $n = 1.076$ describe the Al/Si-rich/SiGe Schottky contact and $\Phi = 0.68$ eV and $n = 1.047$ describe the atomically-sharp SiGe/Al Schottky contact. This confirms the expectation of a slightly lower barrier height for the double-interface contact.

Figure 4 presents the effect of bias on the electron beam induced current. The EBIC response at zero bias, also displayed in figure 3b, is relatively small when compared with the response under bias. Negative bias leads to an enhancement of the current generated in the vicinity of the Al/Si-rich/SiGe interface, whereas positive bias results in enhanced current in the vicinity of the SiGe/Al contact. Each time, the maximum current should be generated in the contact that is reverse biased, which is consistent with the band diagram depicted in figure 3d.

Figure 4b shows the maximum collected current as a function of the beam current, for different bias. Interestingly, the trends show a linear increase of the EBIC current for increasing incident beam current, with the only exception of -4 V bias, which shows signs of saturation. The linearity confirms that we are in a situation of low injection,[24] and other carrier recombination pathways, such as surface traps, have a negligible effect on the EBIC current. The absence of surface effects, which generally lead to a sublinear increase of the collected current as a function of the excitation, demonstrates the efficiency of the surface passivation of the NW obtained by Al_2O_3 encapsulation.

Figure 5a plots the maximum collected current at both interfaces (absolute value) as a function of bias, for an incident beam current of 7 nA. Figure 5b plots the variation of the depletion zone extension as a function of bias for both contacts extracted from the shape of the peak in the EBIC

intensity profiles as described in Supplementary Material Section 2. Under low positive bias, the depletion zone width for the SiGe single interface (reverse biased contact) is 80-98 nm and then gradually extends for increasing positive bias. However, under a low positive bias the depletion zone at the Si-rich interface (reverse biased contact) is only 40-50 nm. This is the approximate width of the Si-rich region (40 nm), implying that the space-charge region is confined here for a reverse bias below 2 V. Above this threshold the depletion zone is able to extend much further into the SiGe material, reaching widths only slightly smaller than those of the SiGe single interface. This evolution could be explained by the Si-rich region being slightly more doped than the SiGe NW, or by the presence of charge states at the Si/SiGe heterointerface. However, the latter explanation seems less probable since microscopy images with atomic resolution show that the Si/SiGe interface does not contain structural defects.

Measurements of the effective diffusion length of minority carriers are plotted in figure 5c, extracted from the EBIC intensity profiles by least-squares fitting an exponential equation to the diffusion region near the depletion zone (see Supporting Material 2).[15] For low positive bias, the measured diffusion length of carriers in the vicinity of the Si-rich interface is only 70-130 nm, whilst it remains around 200-240 nm for bias higher than 2 V, i.e. when the depletion region penetrates the SiGe. Consistently, diffusion lengths around 250 nm are measured at the SiGe interface for all applied bias.

4. Conclusion

We have demonstrated quantitative EBIC of a SiGe nanowire in a STEM instrument, taking advantage of the highly localized generation of charge carriers when using an 80 kV transmission electron beam. High resolution EBIC maps were obtained, despite the presence of a thick insulating SiN_x membrane which prevents other field mapping techniques such as electron holography and differential phase contrast from being successfully used.[43] The SiGe nanowire contains two semiconductor-metal interfaces which act as opposing Schottky contacts, as confirmed by current-voltage measurements. Using high-resolution HAADF STEM imaging, the two contacts were found to be dissimilar: one a single atomically-sharp interface of Al/SiGe, the other a double interface of Al/Si-rich/SiGe. From EBIC measurements, the intrinsic doping of the SiGe semiconductor was determined to be *n*-type. The contacts react linearly under varying electron beam current in the current range under study, confirming that our measurements are performed in low injection conditions and surface effects are not relevant. Analysis of the STEM EBIC intensity profiles revealed that the behaviour of the two contacts under reverse bias is very different. The Si-rich region at the double interface delays the propagation of the depletion region with bias and reduces the measured diffusion length of charge carriers. This trend could be explained by the Si-rich region being slightly more doped than the SiGe NW. These results demonstrate that STEM EBIC is a robust and powerful method for mapping electric fields in low-dimensional materials and quantifying electronic properties with nanoscale resolution. Field mapping by STEM EBIC has now been demonstrated in both NWs and focused ion beam-prepared specimens[42] and should prove to be of great use to the semiconductor community.

Acknowledgements

This work, done on the NanoCharacterisation PlatForm (PFNC), was supported by the "Recherches Technologiques de Base" Program of the French Ministry of Research. We acknowledge financial support of the Cross-Disciplinary Program on Instrumentation and Detection of CEA, the French Alternative Energies and Atomic Energy Commission.

Data availability statement

The data that support the findings of this study are available from the corresponding author upon reasonable request.

ORCID iDs

Aidan Conlan: 0000-0002-1333-9359

Martien den Hertog: 0000-0003-0781-9249

Eva Monroy: 0000-0001-5481-3267

David Cooper: 0000-0003-3479-4374

References

(1) Otnes, G.; Borgström, M. T. Towards High Efficiency Nanowire Solar Cells. *Nano Today* **2017**, *12*, 31–45. https://doi.org/10.1016/j.nantod.2016.10.007.

(2) Burchhart, T.; Lugstein, A.; Hyun, Y. J.; Hochleitner, G.; Bertagnolli, E. Atomic Scale Alignment of Copper-Germanide Contacts for Ge Nanowire Metal Oxide Field Effect Transistors. *Nano Lett.* **2009**, *9* (11), 3739–3742. https://doi.org/10.1021/nl9019243.

(3) Dellas, N. S.; Minassian, S.; Redwing, J. M.; Mohney, S. E. Formation of Nickel Germanide Contacts to Ge Nanowires. *Appl. Phys. Lett.* **2010**, *97* (26), 263116. https://doi.org/10.1063/1.3533808.

(4) Liu, B.; Wang, Y.; Dilts, S.; Mayer, T. S.; Mohney, S. E. Silicidation of Silicon Nanowires by Platinum. *Nano Lett.* **2007**, *7* (3), 818–824. https://doi.org/10.1021/nl062393r.

(5) El hajraoui, K.; Luong, M. A.; Robin, E.; Brunbauer, F.; Zeiner, C.; Lugstein, A.; Gentile, P.; Rouvière, J.-L.; Den Hertog, M. In Situ Transmission Electron Microscopy Analysis of Aluminum–Germanium Nanowire Solid-State Reaction. *Nano Lett.* **2019**, *19* (5), 2897–2904. https://doi.org/10.1021/acs.nanolett.8b05171.

(6) Sistani, M.; Staudinger, P.; Greil, J.; Holzbauer, M.; Detz, H.; Bertagnolli, E.; Lugstein, A. Room-Temperature Quantum Ballistic Transport in Monolithic Ultrascaled Al–Ge–Al Nanowire Heterostructures. *Nano Lett.* **2017**, *17* (8), 4556–4561. https://doi.org/10.1021/acs.nanolett.7b00425.

(7) Sistani, M.; Delaforce, J.; Kramer, R. B. G.; Roch, N.; Luong, M. A.; den Hertog, M. I.; Robin, E.; Smoliner, J.; Yao, J.; Lieber, C. M.; Naud, C.; Lugstein, A.; Buisson, O. Highly Transparent Contacts to the 1D Hole Gas in Ultrascaled Ge/Si Core/Shell Nanowires. *ACS Nano* **2019**, *13* (12), 14145–14151. https://doi.org/10.1021/acsnano.9b06809.

(8) Luong, M. A.; Robin, E.; Pauc, N.; Gentile, P.; Sistani, M.; Lugstein, A.; Spies, M.; Fernandez, B.; Den Hertog, M. I. In-Situ Transmission Electron Microscopy Imaging of Aluminum Diffusion in Germanium Nanowires for the Fabrication of Sub-10 Nm Ge Quantum Disks. *ACS Appl. Nano Mater.* **2020**, *3* (2), 1891–1899. https://doi.org/10.1021/acsanm.9b02564.

(9) Kral, S.; Zeiner, C.; Stöger-Pollach, M.; Bertagnolli, E.; den Hertog, M. I.; Lopez-Haro, M.; Robin, E.; El Hajraoui, K.; Lugstein, A. Abrupt Schottky Junctions in Al/Ge Nanowire Heterostructures. *Nano Lett.* **2015**, *15* (7), 4783–4787. https://doi.org/10.1021/acs.nanolett.5b01748.

(10) Luong, M. A.; Robin, E.; Pauc, N.; Gentile, P.; Baron, T.; Salem, B.; Sistani, M.; Lugstein, A.; Spies, M.; Fernandez, B.; den Hertog, M. Reversible Al Propagation in SixGe1–x Nanowires: Implications for Electrical Contact Formation. *ACS Appl. Nano Mater.* **2020**. https://doi.org/10.1021/acsanm.0c02303.

(11) *Scanning Transmission Electron Microscopy: Imaging and Analysis*; Pennycook, S. J., Nellist, P. D., Eds.; Springer-Verlag: New York, 2011. https://doi.org/10.1007/978-1-4419-7200-2.

(12) *Transmission Electron Microscopy Characterization of Nanomaterials*; Kumar, C. S. S. R., Ed.; Springer-Verlag: Berlin Heidelberg, 2014. https://doi.org/10.1007/978-3-642-38934-4.

(13) Tian, B.; Zheng, X.; Kempa, T. J.; Fang, Y.; Yu, N.; Yu, G.; Huang, J.; Lieber, C. M. Coaxial Silicon Nanowires as Solar Cells and Nanoelectronic Power Sources. *Nature* **2007**, *449* (7164), 885–889. https://doi.org/10.1038/nature06181.

(14) Leamy, H. J. Charge Collection Scanning Electron Microscopy. *J. Appl. Phys.* **1982**, *53* (6), R51–R80. https://doi.org/10.1063/1.331667.
(15) Moldovan, G.; Kazemian, P.; Edwards, P. R.; Ong, V. K. S.; Kurniawan, O.; Humphreys, C. J. Low-Voltage Cross-Sectional EBIC for Characterisation of GaN-Based Light Emitting Devices. *Ultramicroscopy* **2007**, *107* (4), 382–389. https://doi.org/10.1016/j.ultramic.2006.10.002.
(16) Donatini, F.; de Luna Bugallo, A.; Tchoulfian, P.; Chicot, G.; Sartel, C.; Sallet, V.; Pernot, J. Comparison of Three E-Beam Techniques for Electric Field Imaging and Carrier Diffusion Length Measurement on the Same Nanowires. *Nano Lett.* **2016**, *16* (5), 2938–2944. https://doi.org/10.1021/acs.nanolett.5b04710.
(17) Neplokh, V.; Ali, A.; Julien, F. H.; Foldyna, M.; Mukhin, I.; Cirlin, G.; Harmand, J.-C.; Gogneau, N.; Tchernycheva, M. Electron Beam Induced Current Microscopy Investigation of GaN Nanowire Arrays Grown on Si Substrates. *Mater. Sci. Semicond. Process.* **2016**, *55*, 72–78. https://doi.org/10.1016/j.mssp.2016.03.002.
(18) Spies, M.; den Hertog, M. I.; Hille, P.; Schörmann, J.; Polaczyński, J.; Gayral, B.; Eickhoff, M.; Monroy, E.; Lähnemann, J. Bias-Controlled Spectral Response in GaN/AlN Single-Nanowire Ultraviolet Photodetectors. *Nano Lett.* **2017**, *17* (7), 4231–4239. https://doi.org/10.1021/acs.nanolett.7b01118.
(19) Cuesta, S.; Spies, M.; Boureau, V.; Donatini, F.; Hocevar, M.; den Hertog, M. I.; Monroy, E. Effect of Bias on the Response of GaN Axial p–n Junction Single-Nanowire Photodetectors. *Nano Lett.* **2019**, *19* (8), 5506–5514. https://doi.org/10.1021/acs.nanolett.9b02040.
(20) Maximenko, S. I.; Lumb, M. P.; Hoheisel, R.; Gonzalez, M.; Scheiman, D. A.; Messenger, S. R.; Tibbits, T. N. D.; Imaizumi, M.; Ohshima, T.; Sato, S. I.; Jenkins, P. P.; Walters, R. J. Radiation Response of Multi-Quantum Well Solar Cells: Electron-Beam-Induced Current Analysis. *J. Appl. Phys.* **2015**, *118* (24), 245705. https://doi.org/10.1063/1.4939067.
(21) Marcelot, O.; Magnan, P. From EBIC Images to Qualitative Minority Carrier Diffusion Length Maps. *Ultramicroscopy* **2019**, *197*, 23–27. https://doi.org/10.1016/j.ultramic.2018.11.005.
(22) Zhou, R.; Yu, M.; Tweddle, D.; Hamer, P.; Chen, D.; Hallam, B.; Ciesla, A.; Altermatt, P. P.; Wilshaw, P. R.; Bonilla, R. S. Understanding and Optimizing EBIC Pn-Junction Characterization from Modeling Insights. *J. Appl. Phys.* **2020**, *127* (2), 024502. https://doi.org/10.1063/1.5139894.
(23) Gutsche, C.; Niepelt, R.; Gnauck, M.; Lysov, A.; Prost, W.; Ronning, C.; Tegude, F.-J. Direct Determination of Minority Carrier Diffusion Lengths at Axial GaAs Nanowire p–n Junctions. *Nano Lett.* **2012**, *12* (3), 1453–1458. https://doi.org/10.1021/nl204126n.
(24) Tchoulfian, P.; Donatini, F.; Levy, F.; Dussaigne, A.; Ferret, P.; Pernot, J. Direct Imaging of p–n Junction in Core–Shell GaN Wires. *Nano Lett.* **2014**, *14* (6), 3491–3498. https://doi.org/10.1021/nl5010493.
(25) Lavenus, P.; Messanvi, A.; Rigutti, L.; Bugallo, A. D. L.; Zhang, H.; Bayle, F.; Julien, F. H.; Eymery, J.; Durand, C.; Tchernycheva, M. Experimental and Theoretical Analysis of Transport Properties of Core–Shell Wire Light Emitting Diodes Probed by Electron Beam Induced Current Microscopy. *Nanotechnology* **2014**, *25* (25), 255201. https://doi.org/10.1088/0957-4484/25/25/255201.
(26) Tchernycheva, M.; Neplokh, V.; Zhang, H.; Lavenus, P.; Rigutti, L.; Bayle, F.; Julien, F. H.; Babichev, A.; Jacopin, G.; Largeau, L.; Ciechonski, R.; Vescovi, G.; Kryliouk, O. Core–Shell InGaN/GaN Nanowire Light Emitting Diodes Analyzed by Electron Beam Induced Current

Microscopy and Cathodoluminescence Mapping. *Nanoscale* **2015**, *7* (27), 11692–11701. https://doi.org/10.1039/C5NR00623F.
(27) Yang, M.; Dvorak, D.; Leistner, K.; Damm, C.; Watkins, S. P.; Kavanagh, K. L. Axial EBIC Oscillations at Core/Shell GaAs/Fe Nanowire Contacts. *Nanotechnology* **2018**, *30* (2), 025701. https://doi.org/10.1088/1361-6528/aae7fb.
(28) Han, M.-G.; Marshall, M. S. J.; Wu, L.; Schofield, M. A.; Aoki, T.; Twesten, R.; Hoffman, J.; Walker, F. J.; Ahn, C. H.; Zhu, Y. Interface-Induced Nonswitchable Domains in Ferroelectric Thin Films. *Nat. Commun.* **2014**, *5* (1), 1–9. https://doi.org/10.1038/ncomms5693.
(29) Meyer, T.; Kressdorf, B.; Lindner, J.; Peretzki, P.; Roddatis, V.; Jooss, C.; Seibt, M. High-Resolution Scanning Transmission EBIC Analysis of Misfit Dislocations at Perovskite Pn-Heterojunctions. *J. Phys. Conf. Ser.* **2019**, *1190*, 012009. https://doi.org/10.1088/1742-6596/1190/1/012009.
(30) Han, M.-G.; Garlow, J. A.; Marshall, M. S. J.; Tiano, A. L.; Wong, S. S.; Cheong, S.-W.; Walker, F. J.; Ahn, C. H.; Zhu, Y. Electron-Beam-Induced-Current and Active Secondary-Electron Voltage-Contrast with Aberration-Corrected Electron Probes. *Ultramicroscopy* **2017**, *176*, 80–85. https://doi.org/10.1016/j.ultramic.2017.03.028.
(31) Perreault, G. C.; Ast, D. G. A Specimen Stage with No Microscope Modifications Used to Perform EBIC in a STEM. *J. Phys. [E]* **1988**, *21* (12), 1175–1178. https://doi.org/10.1088/0022-3735/21/12/012.
(32) Progl, C. L.; Parish, C. M.; Vitarelli, J. P.; Russell, P. E. Analysis of V Defects in GaN-Based Light Emitting Diodes by Scanning Transmission Electron Microscopy and Electron Beam Induced Current. *Appl. Phys. Lett.* **2008**, *92* (24), 242103. https://doi.org/10.1063/1.2945232.
(33) Mecklenburg, M.; Hubbard, W. A.; Lodico, J. J.; Regan, B. C. Electron Beam-Induced Current Imaging with Two-Angstrom Resolution. *Ultramicroscopy* **2019**, *207*, 112852. https://doi.org/10.1016/j.ultramic.2019.112852.
(34) Chiquito, A. J.; Amorim, C. A.; Berengue, O. M.; Araujo, L. S.; Bernardo, E. P.; Leite, E. R. Back-to-Back Schottky Diodes: The Generalization of the Diode Theory in Analysis and Extraction of Electrical Parameters of Nanodevices. *J. Phys. Condens. Matter* **2012**, *24* (22), 225303. https://doi.org/10.1088/0953-8984/24/22/225303.
(35) Spies, M.; Momtaz, Z. S.; Lähnemann, J.; Luong, M. A.; Fernandez, B.; Fournier, T.; Monroy, E.; Hertog, M. I. den. Correlated and In-Situ Electrical Transmission Electron Microscopy Studies and Related Membrane-Chip Fabrication. *Nanotechnology* **2020**, *31* (47), 472001. https://doi.org/10.1088/1361-6528/ab99f0.
(36) Luong, M. A. Investigation of Al Thermal Diffusion in Ge and SixGe1-x Alloy Nanowires Using in-Situ Transmission Electron Microscopy. PhD thesis, Université Grenoble Alpes, www.theses.fr/2019GREAY050, 2019.
(37) Drouin, D.; Couture, A. R.; Joly, D.; Tastet, X.; Aimez, V.; Gauvin, R. CASINO V2.42—A Fast and Easy-to-Use Modeling Tool for Scanning Electron Microscopy and Microanalysis Users. *Scanning* **2007**, *29* (3), 92–101. https://doi.org/10.1002/sca.20000.
(38) Ashok, S.; Giewont, K. High-Barrier Al/p-Si Schottky Diodes. *IEEE Electron Device Lett.* **1985**, *6* (9), 462–464. https://doi.org/10.1109/EDL.1985.26193.
(39) Duman, S.; Turgut, G.; Ozcelik, F. S.; Gurbulak, B. Electrical Properties of Al/p–Ge and Al/Methyl Green/p–Ge Diodes. *Philos. Mag.* **2015**, *95* (15), 1646–1655. https://doi.org/10.1080/14786435.2015.1042412.

(40) Vali, I. P.; Shetty, P. K.; Mahesha, M. G.; Petwal, V. C.; Dwivedi, J.; Choudhary, R. J. Tuning of Schottky Barrier Height of Al/n-Si by Electron Beam Irradiation. *Appl. Surf. Sci.* **2017**, *407*, 171–176. https://doi.org/10.1016/j.apsusc.2017.02.189.
(41) Lieten, R. R.; Afanas'ev, V. V.; Thoan, N. H.; Degroote, S.; Walukiewicz, W.; Borghs, G. Mechanisms of Schottky Barrier Control on N-Type Germanium Using Ge3N4 Interlayers. *J. Electrochem. Soc.* **2011**, *158* (4), H358. https://doi.org/10.1149/1.3545703.
(42) Conlan, A. P.; Moldovan, G.; Bruas, L.; Monroy, E.; Cooper, D. Electron Beam Induced Current Microscopy of Silicon p–n Junctions in a Scanning Transmission Electron Microscope. *J. Appl. Phys.* **2021**, *129* (13), 135701. https://doi.org/10.1063/5.0040243.
(43) Hertog, M. den; Donatini, F.; McLeod, R.; Monroy, E.; Sartel, C.; Sallet, V.; Pernot, J. In Situ Biasing and Off-Axis Electron Holography of a ZnO Nanowire. *Nanotechnology* **2017**, *29* (2), 025710. https://doi.org/10.1088/1361-6528/aa923c.

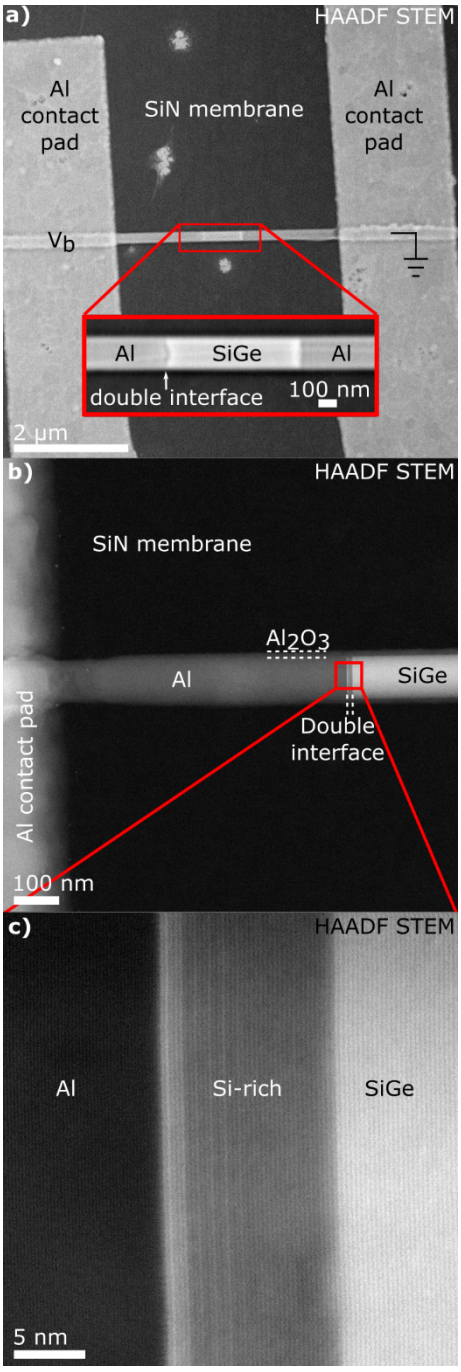

Figure 1. HAADF STEM images showing the structure of the SiGe nanowire / Al interfaces. (a) SiGe nanowire prepared for EBIC on a SiN_x substrate. A double interface with a silicon-rich region is observed at the leftmost contact connected to the amplifier. A sharp Al/SiGe interface is observed at the rightmost contact, connected to earth. (b) and (c) High resolution images of a different nanowire suspended on 40 nm SiN_x. The double interface is crystalline with a silicon rich region separating the SiGe and Al regions of the nanowire.

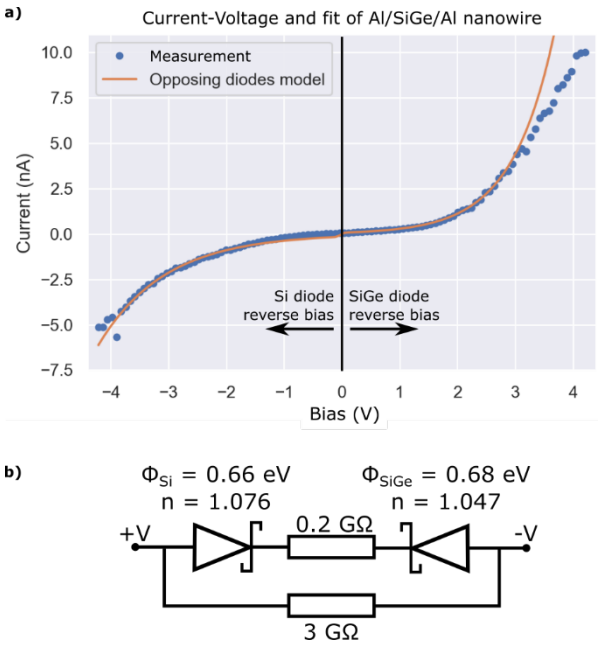

Figure 2. Electrical response of the SiGe nanowire. (a) Current-voltage plot of the nanowire biased from -4 to +4 V (blue), with the opposing Schottky diodes model (orange) plotted for comparison. (b) The values and components used for the opposing diode model.

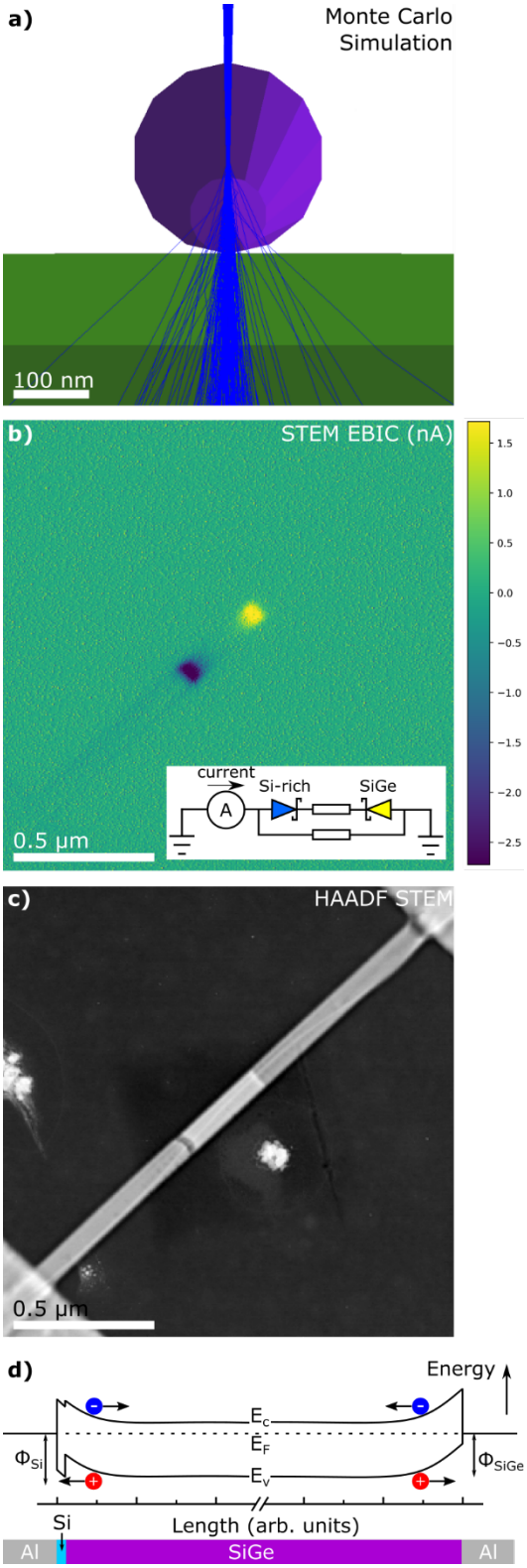
a)
Monte Carlo Simulation
100 nm
b)
STEM EBIC (nA)
0.5 µm
current
Si-rich
SiGe
A
1.5
1.0
0.5
0.0
−0.5
−1.0
−1.5
−2.0
−2.5
c)
HAADF STEM
0.5 µm
d)
Energy
E_c
E_F
E_v
Φ_{Si}
Φ_{SiGe}
Si
Length (arb. units)
Al
SiGe
Al

Figure 3. 80 kV STEM analysis of a SiGe nanowire. (a) Monte Carlo simulation showing the trajectories (blue) of 80 kV electrons in a SiGe nanowire (purple) on a SiN_x substrate (green). (b) STEM EBIC image of the nanowire at zero bias using 1 nA beam current. The two opposing Schottky contacts drive current in opposite directions. Inset: Circuit diagram indicating the current convention. (c) HAADF STEM image of the nanowire acquired simultaneously with EBIC. (d) Band diagram of the NW highlighting the curvature of the bands at the contacts. Electrons (holes) are repelled from (attracted to) the interface in both cases.

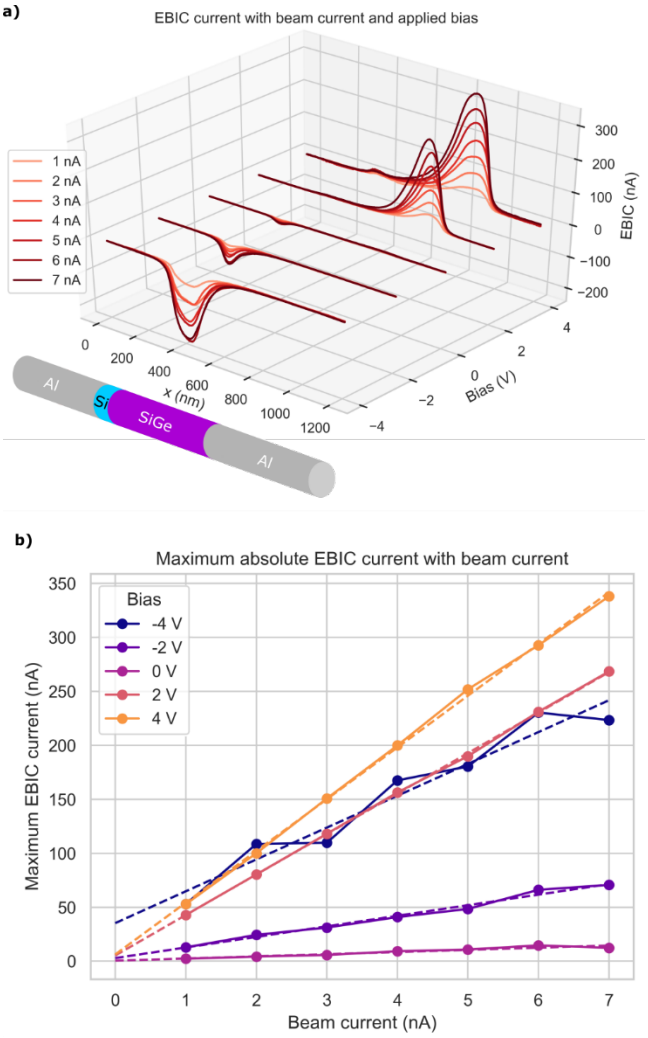

Figure 4. Quantitative STEM EBIC characterization of the SiGe nanowire. (a) STEM EBIC intensity profiles along the nanowire with electron beam current and applied bias. Higher beam currents generate more charge carriers, giving a better signal to noise ratio. (b) Plot of the maximum EBIC values with beam current for different applied bias.

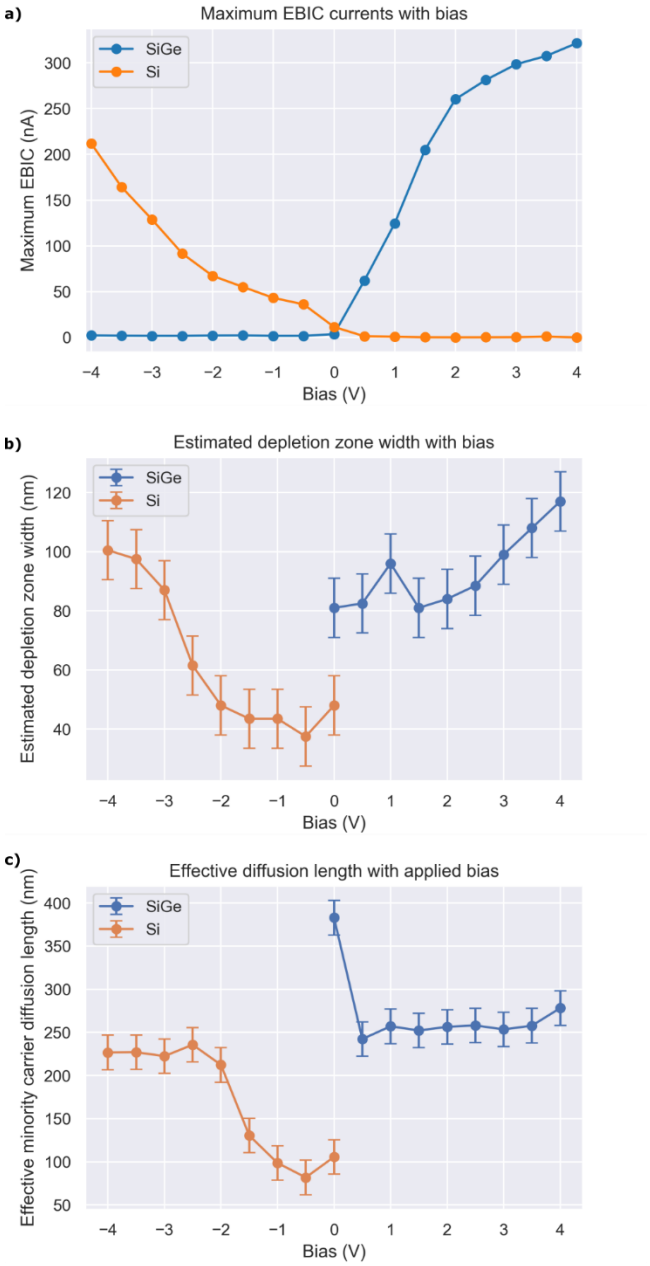

Figure 5. The effect of the double interface on nanowire electrical properties. Each plot shows (a) Maximum EBIC current; (b) estimated depletion zone width; (c) effective diffusion length, with applied bias for the SiGe (blue) and Si-rich (orange) interfaces. The behaviour for both interfaces is very similar above 2 V reverse bias, however below 2 V it is quite different. At low reverse bias the depletion zone is confined within the Si-rich region, however if it is extended into the SiGe region the charge carriers behave as if the interfaces were identical.

CONTENTS FIGURE

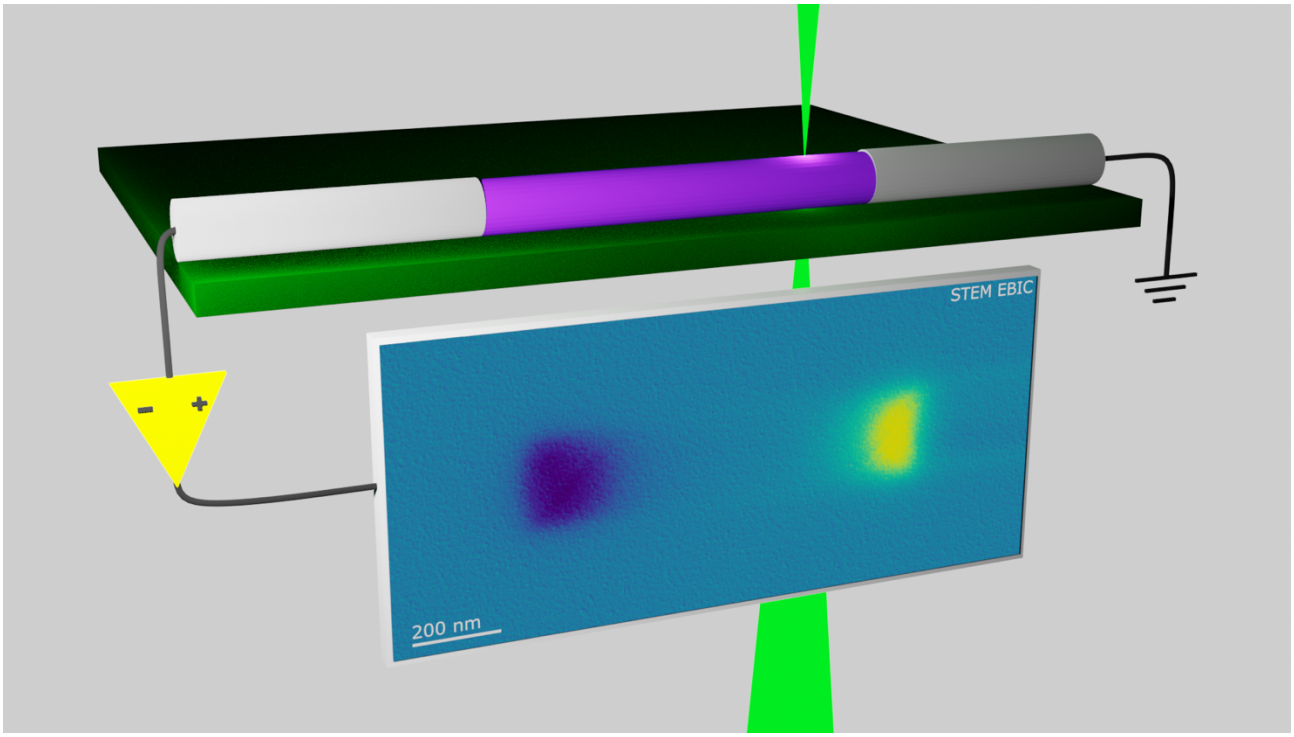

Supplementary Material:

Thermally propagated Al contacts on SiGe nanowires characterized by electron beam induced current in a scanning transmission electron microscope

Aidan P Conlan*[1], Minh Anh Luong[2], Pascal Gentile[3], Grigore Moldovan[4], Martien I den Hertog[2], Eva Monroy[3] and David Cooper[1]

[1] Univ. Grenoble Alpes, CEA-LETI, F-38000 Grenoble, France

[2] Univ. Grenoble Alpes, CNRS-Institut Néel, 25 avenue des Martyrs, F-38000 Grenoble, France

[3] Univ. Grenoble Alpes, CEA, Grenoble INP, IRIG, PHELIQS, 17 av. des Martyrs, F-38000 Grenoble, France

[4] point electronic GmbH, Erich-Neuss-Weg 15, D-06120 Halle (Saale), Germany

Section 1: Structural and chemical characterisation

In Fig. S1 the nanowire (NW) is analysed by high-resolution high-angle annular dark field scanning transmission microscopy (HR-HAADF-STEM) combined with the geometrical phase analysis (GPA) technique. GPA has the advantage over selected area electron diffraction (SAED) that averaging is performed numerically and differences in lattice spacing can be resolved at nanometer length scales.

In Fig. S1a, a HR-STEM image was taken by orienting the propagated NW perpendicular to the electron beam direction in the TEM microscope (Figure S1a). The corresponding Fourier fast transform (FFT) image shown in the inset of Fig. S1b clearly demonstrates the growth direction of the contacted NW, which is along the [111] planes of SiGe. The thermal propagation of Al into the contacted SiGe NW results in the formation of a double interface region with an intermediate contrast, as can be seen in the HAADF image (Fig. S1b), sandwiched between the unreacted SiGe and propagated Al region. The created structure shows an epitaxial alignment of Al(111)//Si-rich(111) and Si-rich(111)//$Si_{0.67}Ge_{0.33}$(111) planes. From GPA analysis, shown in figure 1c-e, the left side in figure 1e shows an average lattice spacing of about 0.321 nm, which demonstrates a chemical combination of Si(111) planes (d=0.313nm) and Ge(111) planes (d=0.327nm). The double interface region in the middle shows an average spacing of 0.315nm, which is close to the spacing of a pure Si compound.

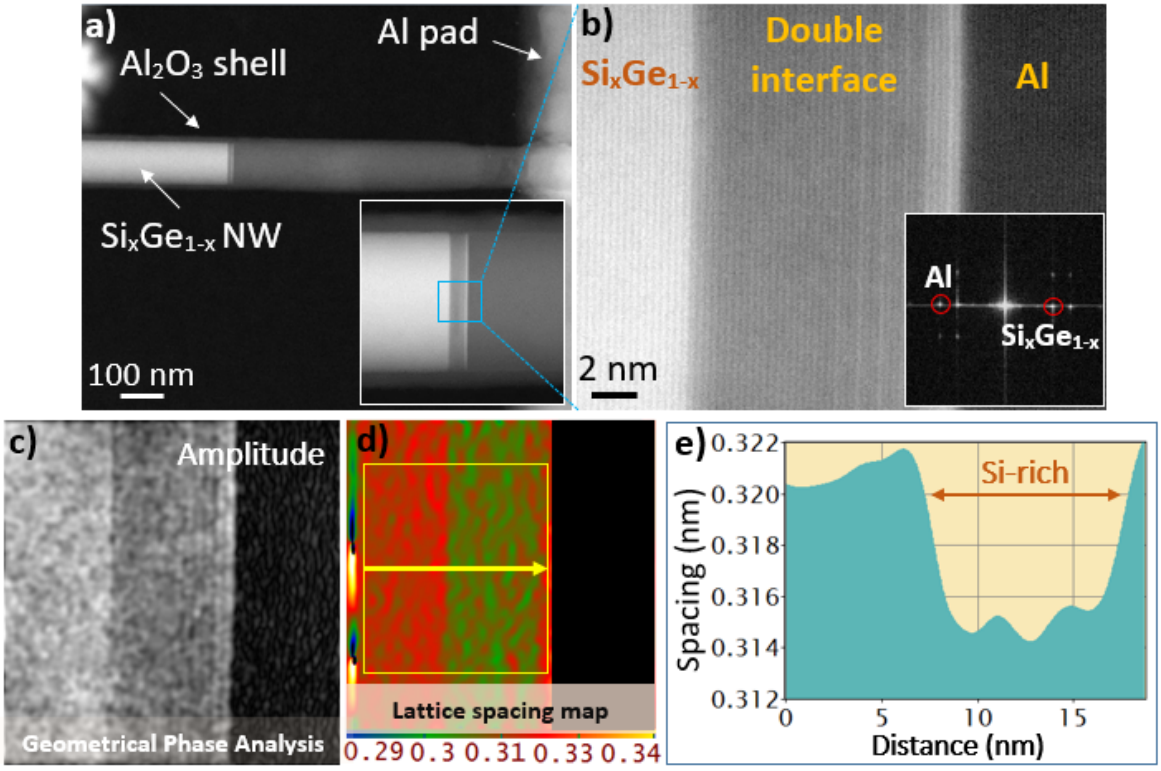

Figure S1: a) HAADF STEM image of the Al contacted $Si_{0.67}Ge_{0.33}$ NW lying on the 200 nm thick Si_3N_4 membrane. The contacted NW was annealed by rapid thermal annealing (RTA) at 450˚C for 20 s in N_2 ambience. **b)** A low field of view HAADF STEM image at the propagated interface showing the formation of a double interface region between the reacted and unreacted parts of the propagated NW. c-e) The extracted amplitude, lattice spacing map and lattice spacing profile using geometrical phase analysis (GPA) on the HR STEM image, showing the lattice spacing profile obtained from a line-scan on the yellow rectangular box in figure 1d.

In addition, a detailed analysis of the NW stoichiometry of the same set of as-grown NWs has been reported in the ref 10 (Luong et al. ACS Appl. Nano Mater. 2020, 3, 10, 10427–10436) and ref 36. In particular, a 3D reconstruction method of the NW cross-section in combination with the zeta factor method has been employed to retrieve the cross-sectional chemical distribution of the propagated NW, which gave us a chemical stoichiometry of $Si_{0.67}Ge_{0.33}$ for the as-grown NWs. A detailed description for the basic steps of the 3D reconstructions can be found in the supporting information of reference 10:
https://pubs.acs.org/doi/suppl/10.1021/acsanm.0c02303/suppl_file/an0c02303_si_001.pdf

Section 2: Determining the effective minority carrier diffusion length from electron beam induced current intensity profiles

Figure S2 summarizes the procedure for extracting the effective minority carrier diffusion length from an electron beam induced current (EBIC) intensity profile. It is known that the variations in EBIC current I_{EBIC} near the edge of the depletion region can be described by:

$$I_{EBIC} = kx^{\alpha}e^{\left(-\frac{x}{L}\right)} \quad \text{(S1)}$$

where x is the distance from the edge of the depletion zone, L is the diffusion length of minority carriers, and k and α are fitting constants [1,2]. Neglecting concavity ($\alpha = 0$), a linear form of the equation is found:

$$\log(I_{EBIC}) = -x\frac{1}{L} + \log(k) \quad \text{(S2)}$$

Figure S2(a) shows the EBIC current recorded at the Si-rich contact at zero bias, and figure S2(b) shows the same data in semi-logarithmic scale. By fitting equation S2 by least squares to the shoulder of the EBIC intensity profile (figure S2c), the diffusion length can be determined.

We observed that $\log(I_{EBIC})$ significantly diverges from linearity when the EBIC intensity is above 80% of the peak maximum. This is to be expected as, for the highest EBIC intensities, we enter the depletion region where the collection of charge carriers is dominated by a drift current in the presence of an electrostatic field, and not by diffusion of minority charge carriers into the depletion region. Therefore, the length of the depletion zone was estimated from the width of the peak at 80% of the peak height for each applied reverse bias, as shown in figure S2d. The results if this analysis are presented in figures 5b and c of the main text.

References

[1] Moldovan G, Kazemian P, Edwards P R, Ong V K S, Kurniawan O, and Humphreys C J 2017 *Ultramicroscopy* **107** 238

[2] Tan C C, Ong V K S, Radhakrishnan K, and Sunar S H S 2013 *IEEE Trans. Electron Devices* **60** 3541

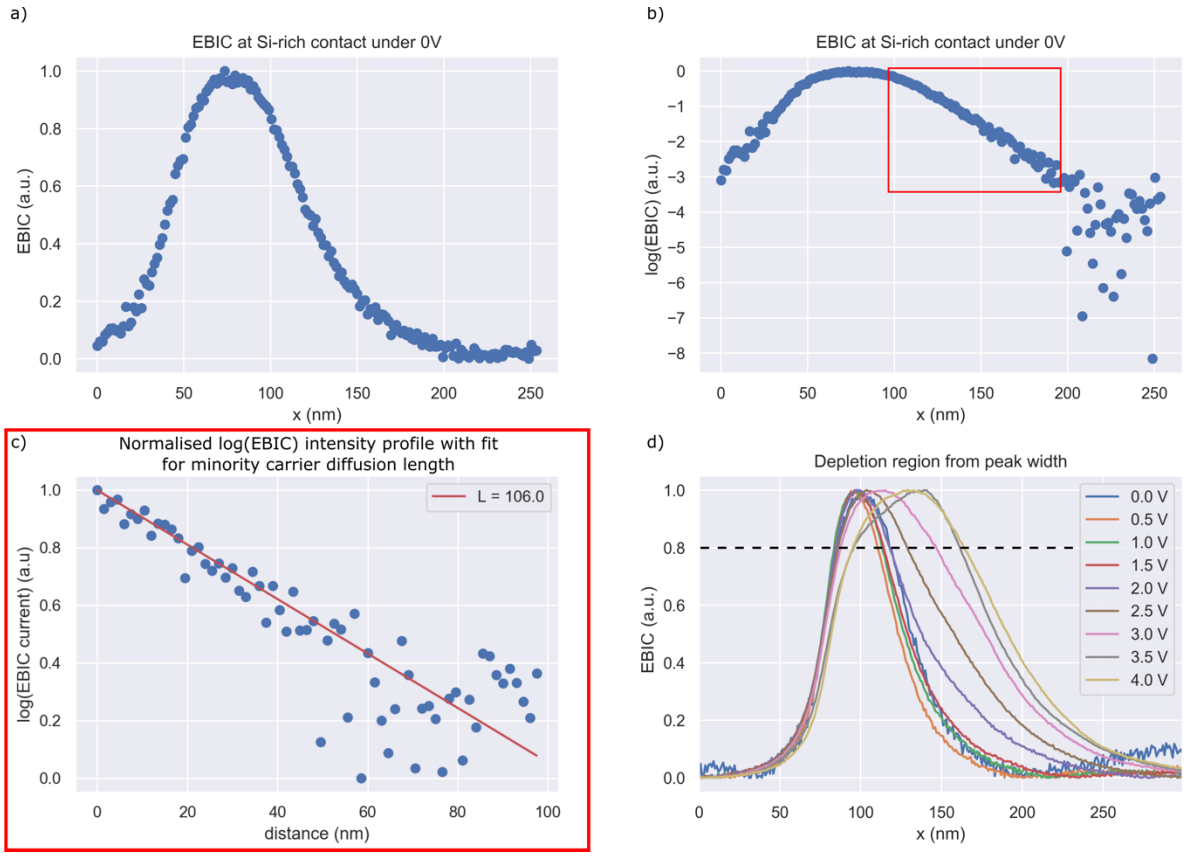

Figure S2. Procedure for extracting the effective minority carrier diffusion length and depletion region width from EBIC intensity profiles. (a) EBIC intensity profile for the Si-rich contact under zero bias and (b), replotted with a log scaled y-axis. The linear section of the trend within the red box is shown normalized in (c). By finding the gradient of this trend the effective diffusion length of minority carriers can be determined. (d) A plot showing the change in peak shape of the EBIC intensity profiles with applied reverse bias. The length of the depletion region is estimated by extracting the width of the peak at 80% of the maximum EBIC intensity. The fit of the diffusion length fails to describe the EBIC profile above this value, showing that the charge carriers obey a drift current in an electrostatic field.